



HAL
open science

Imperfect automatic image classification successfully describes plankton distribution patterns

Robin Faillettaz, Marc Picheral, Jessica Y. Luo, Cédric Guigand, Robert K. Cowen, Jean-Olivier Irisson

► **To cite this version:**

Robin Faillettaz, Marc Picheral, Jessica Y. Luo, Cédric Guigand, Robert K. Cowen, et al.. Imperfect automatic image classification successfully describes plankton distribution patterns. *Methods in Oceanography*, 2016, 10.1016/j.mio.2016.04.003 . hal-01324904

HAL Id: hal-01324904

<https://hal.sorbonne-universite.fr/hal-01324904v1>

Submitted on 1 Jun 2016

HAL is a multi-disciplinary open access archive for the deposit and dissemination of scientific research documents, whether they are published or not. The documents may come from teaching and research institutions in France or abroad, or from public or private research centers.

L'archive ouverte pluridisciplinaire **HAL**, est destinée au dépôt et à la diffusion de documents scientifiques de niveau recherche, publiés ou non, émanant des établissements d'enseignement et de recherche français ou étrangers, des laboratoires publics ou privés.

1 **IMPERFECT AUTOMATIC IMAGE CLASSIFICATION SUCCESSFULLY**
2 **DESCRIBES PLANKTON DISTRIBUTION PATTERNS**

3
4 Robin Faillettaz¹; Marc Picheral¹; Jessica Y. Luo^{2,3}; Cédric Guigand²; Robert K. Cowen^{2,3}; Jean-
5 Olivier Irisson^{1*}

6
7 ¹Sorbonne Universités, UPMC Univ Paris 06, CNRS, Laboratoire d'Océanographie de Villefranche,
8 181 Chemin du Lazaret, 06230 Villefranche-sur-Mer, France

9 ²Marine Biology and Fisheries, Rosenstiel School of Marine and Atmospheric Science (RSMAS),
10 University of Miami, Miami FL 33149, USA

11 ³Oregon State University, Hatfield Marine Science Center, Newport OR 97365, USA

12

13 *Corresponding author: irisson@normalesup.org

14

15 **ABSTRACT**

16 Imaging systems were developed to explore the fine scale distributions of plankton (<10 m), but
17 they generate huge datasets that are still a challenge to handle rapidly and accurately. So far,
18 imaged organisms have been either classified manually or pre-classified by a computer program
19 and later verified by human operators. In this paper, we post-process a computer-generated
20 classification, obtained with the common *ZooProcess* and *PlanktonIdentifier* toolchain
21 developed for the ZooScan, and test whether the same ecological conclusions can be reached
22 with this fully automatic dataset and with a reference, manually sorted, dataset. The Random
23 Forest classifier outputs the probabilities that each object belongs in each class and we discard
24 the objects with uncertain predictions, i.e. under a probability threshold defined based on a 1%
25 error rate in a self-prediction of the learning set. Keeping only well-predicted objects enabled
26 considerable improvements in average precision, 84% for biological groups, at the cost of
27 diminishing recall (by 39% on average). Overall, it increased accuracy by 16%. For most groups,
28 the automatically-predicted distributions were comparable to the reference distributions and
29 resulted in the same size-spectra. Automatically-predicted distributions also resolved
30 ecologically-relevant patterns, such as differences in abundance across a mesoscale front or
31 fine-scale vertical shifts between day and night. This post-processing method is tested on the
32 classification of plankton images through Random Forest here, but is based on basic features
33 shared by all machine learning methods and could thus be used in a broad range of applications.

34 **KEYWORDS**

35 Imaging system; ISIS; Automatic classification; Plankton distribution; Machine learning; Big
36 dataset

37 INTRODUCTION

38 From the centimetre to kilometre-scales, hydrodynamics, predator-prey interactions and
39 behaviour strongly structure the patchy distributions of planktonic organisms in pelagic
40 environments (Davis et al., 1992; Pinel-Alloul, 1995; Lough and Broughton, 2007). At mesoscales
41 (10-100 km) and submesoscales (<10 km), plankton distributions are primarily determined by
42 hydrological structures like fronts and eddies (Belkin, 2002; Belkin et al., 2009; Luo et al., 2014).
43 For example, convergent flows at frontal features can increase primary production (Grimes and
44 Finucane, 1991) and mechanically concentrate organisms (Bakun, 2006; Olson et al., 1994).
45 However, the influence of these structures may be counter-balanced by behaviour or other
46 biotic processes. Indeed, at fine scale (<1 km), diel vertical migrations can be a strong driver of
47 plankton distributions (Benoit-Bird and McManus, 2012; Neilson and Perry, 1990). At
48 microscales (<1 m to 10 m), biotic interactions such as competition and predation are likely to
49 generate vertical gradients in the distribution of zooplankton. For example, in Monterey Bay,
50 predator avoidance is thought to vertically separate copepods, phytoplankton thin layers, and
51 gelatinous zooplankton predators (Greer et al., 2013). Off the coast of Massachusetts,
52 interactions between internal waves and foraging drives a temporary overlap between layers of
53 high copepod concentration and ichthyoplankton (Greer et al., 2014).

54 Historically, zooplankton and ichthyoplankton distributions have been sampled with pumps
55 (Herman et al., 1984) and regular or stratified plankton nets (e.g. regular: WP2, Bongo; e.g.
56 stratified: MOCNESS, BIONESS, MULTINET; Wiebe and Benfield, 2003). However, even depth-
57 stratified nets cannot typically resolve the fine and microscale processes at which biotic
58 interactions occur, because they usually sample (and integrate) over at least 10 m vertically and
59 much more horizontally. While pumps offer finer spatio-temporal resolution, they are often
60 limited to surface layers (<10 m depth -- Boucher, 1984; sometimes down to 100 m depth --
61 Herman et al., 1984) and sample much smaller volumes (on average $50\text{-}60\text{ L min}^{-1}$ vs.
62 $7,500\text{ L min}^{-1}$ for a small plankton net; Wiebe and Benfield, 2003).

63 In the last two decades, *in situ* imaging systems were developed with the aim of sampling

64 microscale processes in the plankton and accelerating data processing using efficient automatic
65 classification techniques (MacLeod et al., 2010; Wiebe and Benfield, 2003). Several imaging
66 systems have emerged, tackling different ecological questions by targeting different size spectra
67 of organisms. The Video Plankton Recorder (VPR; Benfield et al., 1996) and the Underwater
68 Vision Profiler (UVP; Picheral et al., 2010) sample particles and zooplankton. The Shadow Image
69 Particle Profiling Evaluation Recorder (SIPPER; Samson et al., 2001), the ZOOplankton
70 VISualization imaging system (ZOOVIS; Bi et al., 2013) and the *In Situ* Ichthyoplankton Imaging
71 System, used for this study (ISIIS; Cowen and Guigand, 2008), target large zooplankton up to
72 several centimetres. ISIIS has been specifically designed to sample fish larvae that are patchy
73 and rare (Cowen et al., 2013). Therefore, it samples larger volumes of water compared to other
74 instruments (ISIIS: from 108 to 168 L s⁻¹; UVP: typically 8 L s⁻¹, up to 20.0 L s⁻¹; SIPPER 9.2 L s⁻¹;
75 ZOOVIS 3.6 L s⁻¹; VPR: 10 to 17 mL s⁻¹) and has proved to be particularly suited to describe the
76 fine-scale distribution of both ichthyoplankton (Cowen et al., 2013; Greer et al., 2014) and other
77 taxa, including gelatinous zooplankton (Luo et al., 2014; McClatchie et al., 2012). These imaging
78 systems generate large datasets of images. For example, in one hour, ISIIS records over
79 200 billion pixels (the equivalent of more than 200 GB of greyscale TIFF images), usually yielding
80 several hundred thousand objects of interest, that have to be identified. Manually processing
81 such big datasets has to be limited to few groups of interest (e.g. Greer et al., 2015, 2014; Luo et
82 al., 2014; McClatchie et al., 2012) but remains time prohibitive. Developing accurate automatic
83 identification processes for such datasets is still a challenge (Benfield et al., 2007; Cowen et al.,
84 2013; Culverhouse et al., 2006) that needs to be solved in order to fully resolve microscale
85 processes.

86 Imaging data are typically handled in a three-step process: first, detecting and segmenting
87 relevant objects (or regions of interest) from raw images; then measuring features of each
88 object (such as size, aspect ratio, etc.); and finally using these features to classify the objects
89 into biologically/ecologically relevant groups through machine learning algorithms. Several
90 automatic identification procedures have already been tested on plankton datasets of a few
91 thousand images using various classifiers: Random Forest (e.g. Bell and Hopcroft, 2008), Support
92 Vector Machines (e.g. Hu and Davis, 2005), Bayesian models (Ye et al., 2011) or neural networks

93 (e.g. Davis et al., 2004). Some also combined several classifiers to improve prediction accuracy
94 (Hu and Davis, 2005; Li et al., 2014; Zhao et al., 2010). While the algorithms differ, all of these
95 classifiers have in common the fact that they result in a final score (often a probability) for an
96 object to be in *each* class and attribute the object to the class with the highest score. This
97 predicted class is often the only information that is retained from the classifier. So, while
98 classification is typically viewed as a yes-or-no problem, the real outputs from the classifiers are
99 actually continuous.

100 In this study, we take the example of the commonly-used image processing and identification
101 toolchain *ZooProcess* and *Plankton Identifier (PkID)* (Gorsky et al., 2010). The software was first
102 developed for the *ZooScan* (laboratory plankton scanner) and then extended to the UVP
103 (Picheral et al., 2010) and other imaging systems. *ZooProcess* segments objects from the full
104 image and computes a set of descriptive features (grey levels, length, width, area, shape, etc.)
105 that are then used by *PkID* through various classification algorithms (Support Vector Machine,
106 Neural network, Random Forest, etc.), although Random Forest (Breiman, 2001) has proven to
107 be the most accurate and is now used routinely (Gorsky et al., 2010). This software suite is free,
108 open-source, easy to install, and well supported. Therefore, it is widely distributed worldwide
109 and used by 60 research teams from the tropics to the poles (e.g. France (Vandromme et al.,
110 2011); New-Caledonia (Smeti et al., 2015); Antarctica (Espinasse et al., 2012)). It is most
111 commonly used as a *computer-assisted* identification system, whereby the classifier proposes
112 identifications that are then validated by human operators for all objects.

113 *ZooProcess* and *PkID* offer appropriate tools to handle ISIS data but the amount of data
114 generated by ISIS makes human validation impractical. For example, validating the
115 identifications of the 1.5 million objects used as a reference in this study took seven full-time
116 months; a few days of ISIS deployments typically yield from ten to a hundred million objects.
117 However, given the size and spatial resolution of the dataset, even a subset of it is likely to
118 contain relevant ecological information, at least at the meter to 10 m scale. Here, we propose to
119 discard objects with a low classification score (i.e. the least likely to be correctly identified) and
120 assume that all remaining objects are correctly classified, hence bypassing the validation step.

121 Most other studies compare automatic classification methods using only classification metrics
122 (e.g. precision, recall). We suggest that a more biologically relevant approach is to examine
123 whether the same ecological patterns can be detected in datasets generated by various
124 methods. Here we compare the same data either manually identified (hereafter the *reference*
125 dataset) or automatically classified and further filtered based on classification score (hereafter
126 the *predicted* dataset). We specifically explore the fine-scale spatial distribution of zooplankton
127 across a frontal structure, its relationship with the environment, the size distribution of
128 planktonic groups as well as their diel vertical migration patterns.

129 **MATERIALS AND METHODS**

130 *Description of ISIS*

131 The *In Situ* Ichthyoplankton Imaging System (ISIS) is a towed underwater imaging system
132 (Cowen and Guigand, 2008). It uses backlight shadowgraph imaging, which makes it ideally
133 suited for small and often transparent planktonic organisms in a consistent manner. The version
134 of ISIS used here was slightly modified from that of Cowen and Guigand (2008). The line-scan
135 camera imaged a 10.5 cm-tall field of view with a 50 cm depth of field. With a line-scan camera,
136 the image is created by the movement of the instrument and scanning at 28 kHz produced a
137 continuous image when towed at 2 m s^{-1} (4 knots). These settings resulted in a sampling rate of
138 108 L s^{-1} . Additionally, ISIS is equipped with environmental sensors recording temperature,
139 conductivity (hence salinity and density), oxygen, chlorophyll *a* fluorescence and
140 photosynthetically active radiation (PAR) at a rate of 2 Hz.

141 *Test data*

142 ISIS was deployed for two transects across the Ligurian current, a coastal jet that creates a
143 permanent, mesoscale front. The current delineates a coastal, a frontal and an offshore zone,
144 with characteristic hydrological properties (Sammari et al., 1995) and biological communities
145 (Boucher et al., 1987). One transect was conducted at night, the other during the following day,

146 in July 2013. Both transects were conducted on the same line, though the night transect
147 sampled from onshore to offshore, and the day transect sampled from offshore to onshore.
148 Thanks to moveable fins, ISIS sampled the water column in a tow-yo fashion, between the
149 surface and 100 m depth, with a vertical speed of 0.2 m s^{-1} . The images in this study come from
150 13 down-casts of the night transect and 7 down-casts of the day transect, which were the only
151 ones fully processed of the ~26 total up- and down- casts of each transect.

152 *Image pre-processing*

153 ISIS collected a continuous stream of pixels, 2048 pixels in height. The stream was cut into
154 square 2048 x 2048 frames by the acquisition software (example in Figure 1). Because the
155 camera was continuously scanning the same line, a single speckle or scratch along the optical
156 path would create a continuous streak in the resulting 2D image. These streaks were removed
157 by dividing each frame by the average of the previous 50 consecutive frames and normalising
158 the result to [0, 255] in grey intensity, a process known as flat-fielding.

159 *Segmentation*

160 The shadows of planktonic organisms or particles imaged by ISIS appeared dark on a light
161 background. All images were thresholded at the 195 grey level; i.e. adjacent pixels darker than
162 195 (255=white, 0=black) were considered as objects of interest. The flat-fielding procedure
163 resulted in an almost white background and well contrasted objects (Figure 1). Therefore, the
164 detection of objects was not very sensitive to the threshold value and 195 was chosen after a
165 few tests.

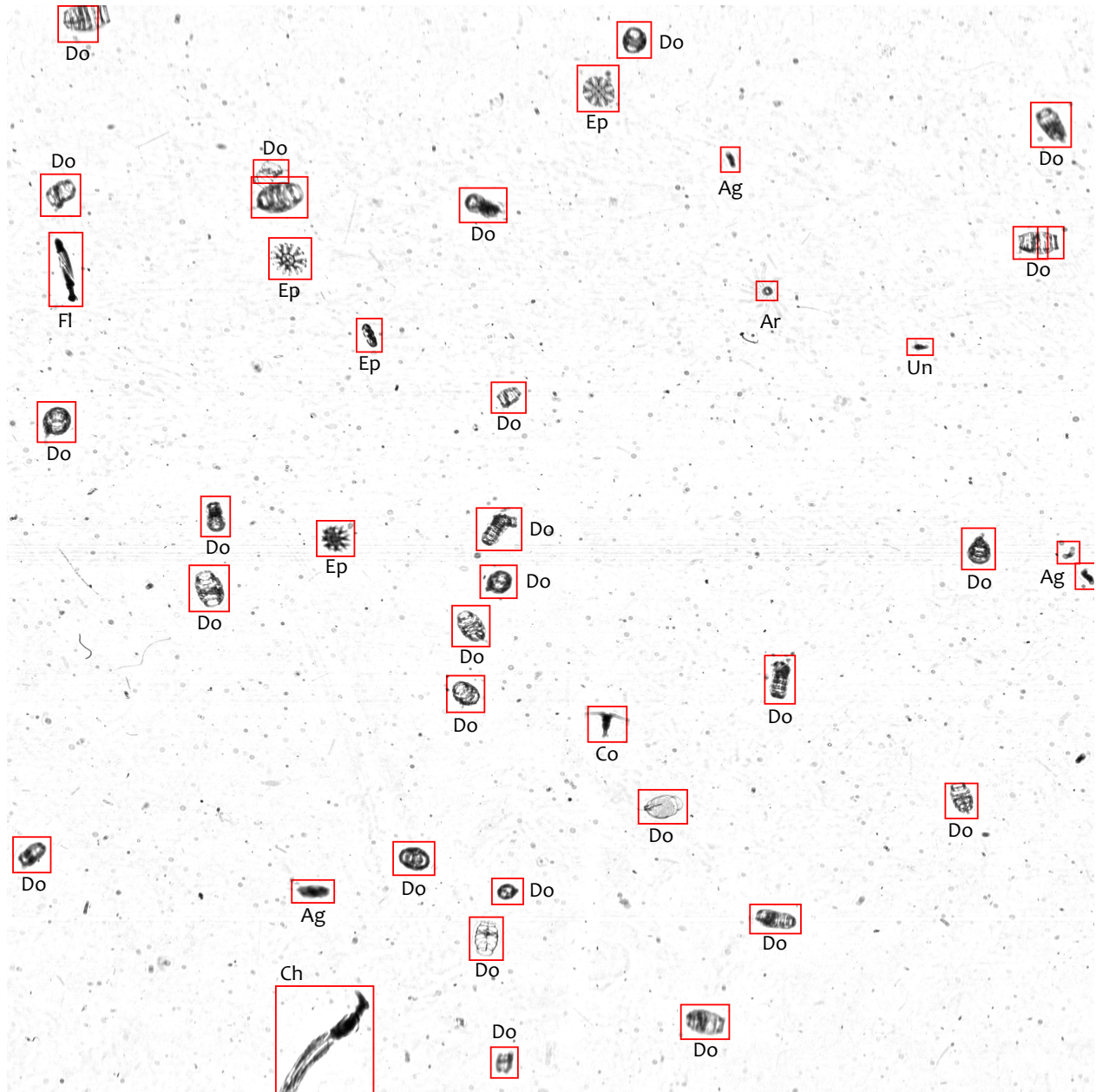
166 Small objects were difficult to identify reliably, even for human operators. Only objects larger
167 than 250 px in area (equivalent to 18 px in diameter for a spherical object) were considered in
168 this study. With a pixel resolution of $51 \mu\text{m}$, this converts to an area of 0.6 mm^2 and an
169 equivalent diameter of $920 \mu\text{m}$.

170 All objects with sufficient size and darkness were segmented out of the frames (Figure 1
171 exemplifies which objects were considered and which were not) and the region outside of the

172 object itself was made pure white. A total of 1.5 million objects were detected.

173 *Feature extraction*

174 The purpose of this study is to optimise an existing classification procedure *a posteriori*.
175 Therefore, the feature extraction was based on the standard configuration in *ZooProcess/PkID*
176 and is not described in detail here (please refer to Gasparini and Antajan, 2013; Gorsky et al.,
177 2010). Briefly, 37 features were measured by *ZooProcess*, and 9 additional variables were
178 derived by *PkID* from the original 37 features. These features characterised each object's size
179 and shape (length of the minor and major axes of the best fitting ellipse, Feret diameter,
180 circularity, symmetry, aspect ratio), transparency (five measures of grey levels: mean, mode,
181 standard deviation, minimum, maximum), and aspect (grey level histogram descriptors such as
182 skewness, cumulative histograms, etc.). When combined, those features can characterise object
183 classes; for example, small, dark, ovoid objects with a large Feret diameter compared to their
184 overall size are probably copepods with their antennae extended. Therefore, they serve as the
185 basis for automatic classification.



186

187 **Figure 1. Example of a flat-fielded 2048 x 2048 pixels frame collected by ISIS.** The bounding
188 box of objects extracted and measured is drawn in red. Those objects are labelled (Ag:
189 aggregates; Ar: Trachymedusae *Arctapodema spp*; Ch: chaetognath; Co: calanoid copepod; Do:
190 doliolid; Ep: *Pelagia noctiluca* ephyrae; Fl: fish larva; Un: unidentified). Note that, on rare
191 occasions, some small-bodied and transparent organisms, such as doliolids, were either
192 truncated or split into several objects and then became hardly identifiable.

193 *Learning set and classification*

194 Supervised classification techniques require a set of identified and measured objects to learn
195 the differences between classes based on their features. Our learning set comprised 14 biotic
196 and abiotic classes with a target size of 200 objects per class (see Table 1), a number which
197 proved to be appropriate for previous *ZooProcess/PkID* projects (Gorsky et al., 2010). The most
198 numerous classes in the data (noise in particular) were also inflated in the learning set, to get a
199 total of 5979 objects. Objects in the learning set were chosen to be representative of the
200 diversity of each class.

201 All 1.5 million segmented objects were classified into these 14 classes by a Random Forest
202 classifier using the 46 measured features (Gorsky et al., 2010). The parameters of the classifier
203 were left at the appropriate defaults in *PkID*: 100 trees, bagging of 1, 6 features randomly
204 selected per tree, leaf size of 2 objects.

205 Finally, three trained operators validated the classification of each object, yielding a completely
206 manually-identified dataset of 1.5 million objects, hereafter referred to as the *reference* dataset.

207 **Table 1. Name, number of objects in the learning set (n) and description of classes.** First non-
208 living objects or artefacts, then biological organisms.

Class	n	Description, taxonomical identification
Dark aggregates	314	Solid, opaque marine snow
Light aggregates	489	Marine snow (larvacean houses, mucus, etc.)
Fibers	433	Thin fibers and fecal pellets
Noise	2296	Noise generated by water density changes
Tentacles	224	<i>Pelagia noctiluca</i> tentacles
Copepods	349	Mainly calanoid copepods
Doliolids	209	Thaliacean, Family Doliolidae
Fish larvae	289	Fish larvae
Trachymedusae	200	Trachymedusae (e.g. <i>Arctapodema spp</i>)
Diatom chains	342	Phytoplankton, diatoms chains

Acantharia radiolarians	213	Radiolaria, Order Acantharia
Radiolarian colonies	255	Radiolaria, Order Colodaria, in colonies
Solitary radiolarians	267	Radiolaria, Order Colodaria, solitary
Shrimps	99	Shrimp-like organisms (e.g. Mysidaceae or Euphausiacea)

209 *Data filtering and optimisation of the classifier precision*

210 To detect meaningful ecological patterns in the distribution of a computer-predicted class, there
211 needs to be sufficiently high confidence that objects in that class belong to the same taxonomic
212 group. In terms of classifier performance, this requires high *precision* (precision = proportion of
213 correctly classified objects in a predicted class). With low precision, a predicted class would be a
214 heterogeneous mixture of various taxonomic groups, the distribution of which cannot be
215 interpreted ecologically. Conversely, for high frequency imaging datasets, the data are often in
216 sufficient quantity that a subsample of the whole dataset would be enough for detecting
217 ecological patterns. In terms of classification metrics, a low *recall* may be acceptable (recall =
218 proportion of the total number of objects of a class that are predicted in that class). Therefore,
219 we suggest that, to detect ecological patterns in a high frequency dataset, particularly for
220 common taxa, precision is more important than recall. To test this hypothesis, we filtered out
221 the most likely mistakes in the computer-predicted dataset (to increase precision), at the cost of
222 discarding some correctly identified objects (hence decreasing recall), and then compared the
223 resulting dataset against the reference set.

224 The probabilities for each object to be in each class (i.e. the final output of the classifier) were
225 used as the filtering criterion. All objects assigned to a given class were ranked in increasing
226 order of probability. All objects with probability above a threshold were kept and assumed to be
227 correctly identified; other objects, with probability equal to or lower than the threshold, were
228 considered to be potentially wrong and were discarded. Since precision needs to be controlled,
229 the threshold should be set to result in a given precision. For example, picking the probability of
230 the first wrongly identified object as the threshold would yield 100% precision (all objects
231 ranked above the first false positive are correctly classified). Here, a 1% error rate (99%
232 precision) was deemed acceptable. Error rates lower than 1% resulted in discarding 3% more

233 objects while improving precision by only 0.2. Higher error thresholds resulted in low precision
234 when applied to the whole dataset (average precision with threshold at 10%=54, at 5%=60.1, at
235 1%=76.9). A 1% error threshold allowed us to increase precision significantly and still keep a
236 representative percentage of objects.

237 The computation of thresholds was done with the learning set only, because in operational
238 conditions, only the identifications of the objects in the learning set are known. The class
239 probability of each object in the learning set was predicted using 2-fold cross-validation
240 repeated 50 times, using the Random Forest classifier in PkID. The probabilities were averaged
241 over the 50 repetitions, objects were assigned to the class of highest probability, and probability
242 thresholds at 1% error were computed in each class. Those thresholds, computed on the
243 learning set, were then applied to the predictions of the 1.5 million objects and the subset of
244 objects that was kept constituted the *predicted* dataset. Thus, once the objects in the learning
245 set are identified manually (which is required for prediction anyway), this precision optimisation
246 method requires only computation, no further human validation effort.

247 *Consequence of data filtering on classification metrics*

248 By construction, the chosen thresholds resulted in exactly 99% precision on the learning set.
249 Because all 1.5 million objects in the reference set were actually identified in this exercise, the
250 precision, recall and F1 score ($2 \times \text{precision} \times \text{recall} / (\text{precision} + \text{recall})$) could be computed for
251 each class over the whole dataset, before and after the filtering process. This allowed us to
252 check whether the precision after filtering approached 99% on the whole dataset as well and
253 how much this improvement in precision cost in terms of decrease in recall.

254 *Comparison of size spectra*

255 The size structure of planktonic communities is often considered as a proxy to study the transfer
256 of energy through the food web and the export and sequestration of carbon (Legendre and Le
257 Fèvre, 1991). It could be expected that smaller objects would be less defined, would therefore
258 be predicted with lower confidence (i.e., lower probabilities) and may be preferentially filtered
259 out by our method. To assess this, size spectra (i.e., probability density distributions of sizes)

260 were estimated with a kernel method (Gaussian kernel with a 0.25 mm standard deviation) and
261 compared in the reference and predicted dataset.

262 *Statistical comparisons of spatial distributions*

263 Individual objects were counted over 1 m depth bins along the undulating trajectory of ISIS and
264 counts were transformed into concentrations by dividing by the volume sampled in each bin.
265 This resulted in maps of the concentration of each class of organism across depth (0-100 m) and
266 distance from the coast (0-60 km) for each transect (for examples see Figures 3 and 4).

267 The similarity between the maps for the reference and predicted datasets was assessed using
268 the t -test modified by Dutilleul (Dutilleul et al., 1993; H0: no correlation between the maps, H1:
269 significant correlation between the maps), as well as the Pearson and Spearman correlation
270 coefficients. On a map, observations close to each other are usually similar; this spatial
271 autocorrelation means that observations close to each other are not independent and that the
272 number of actual degrees of freedom is lower than the apparent sample size. The Dutilleul t -test
273 corrects the number of degrees of freedom based on the spatial autocorrelation of the data
274 (computed as Moran's I) and is therefore appropriate to avoid over-estimating the similarity of
275 spatial patterns.

276 Because diel-vertical migration is such a widespread behaviour in marine ecosystems (Hays,
277 2003) and strongly influences survival through predator-avoidance and foraging in many taxa
278 (Neilson and Perry, 1990), data were specifically inspected in the vertical dimension. Average
279 vertical distributions were computed for each group and each transect (hence separating day
280 and night). Reference and predicted vertical distributions were compared with the version of
281 Kolmogorov-Smirnoff test modified by Solow et al. (2000), which specifically takes into account
282 autocorrelation along depth caused by the patchiness of plankton.

283 By construction, concentrations were lower in the predicted dataset than in the reference
284 dataset, because the former is a subset of the latter. Before the comparisons described above,
285 concentrations were normalised to a maximum value of 1 for each class in each transect, by
286 dividing by the maximum concentration recorded. This put the focus on distribution patterns,

287 rather than actual concentration values, which were poorly estimated when recall was low
288 anyway.

289 Finally, the predicted and reference datasets are not independent (one is a subset of the other)
290 and the absolute values of the test statistics and p -values are therefore biased. The relative
291 values, among classes, are informative however.

292 *Comparison of ecological patterns*

293 The frontal structure across which the transects were sampled is characterised by an inshore-
294 offshore gradient of increasing salinity, with a front that can be delineated by the 38.2 and 38.3
295 isohalines (Sammari et al., 1995) and is expected to strongly structure zooplankton communities
296 (e.g. Boucher, 1984; Pedrotti and Fenaux, 1992). Beyond comparing the distribution maps for
297 the reference and predicted datasets statistically, the results were interpreted with respect to
298 the frontal structure to check whether the ecological patterns were the same. In addition, the
299 relationships between planktonic abundances and environmental variables were inspected in
300 the reference and predicted datasets. The variables inspected were: salinity, which best marks
301 the front, temperature, which is strongly stratified vertically, chlorophyll a fluorescence, which
302 marks a clear Deep Chlorophyll Maximum (DCM), and oxygen concentration, which depends
303 both on the frontal structure and on the DCM. When the relationships could be considered
304 linear, the slopes were estimated through Generalised Linear Models (GLM) with Poisson errors
305 and statistically compared between the two datasets using ANOVA.

306 Similarly, beyond comparing vertical distributions statistically, we assessed whether the range
307 and strength of diel vertical migrations could be as readily detected in the predicted dataset
308 than in the reference dataset. Within each class, day and night distributions were compared
309 with the Solow-Kolmogorov-Smirnov test and the value of its statistic was compared between
310 reference and predicted data. The day-night shift in the depth centre of mass of the
311 distributions (mean of depth weighted by abundance at that depth, Z_{cm} ; Irisson et al., 2010) was
312 computed and compared between the reference and predicted datasets.

313 *Data selection*

314 Abrupt changes in water temperature around the thermocline generated large density
315 differences, which are unfortunately well captured on shadowgraphs. These numerous objects
316 (n=1,287,302) were classified as "Noise". Another abundant class of objects were tentacles of
317 the medusa *Pelagia noctiluca* (n=8,106), which occasionally got stuck on ISIS and were imaged
318 constantly. These two classes of objects are not biologically relevant in the present study, but
319 were abundant and predicted with high precision (>95%), and were thus both omitted from the
320 subsequent analyses.

321 **RESULTS**

322 *Consequences of data filtering on classification metrics*

323 Discarding low probability images considerably increased precision, by 37% on average (Table
324 2). While probability thresholds were set to yield 99% precision on the cross-validated learning
325 set, precision was lower when the thresholds were applied to the whole dataset. This was
326 expected, because the ~6000 images in the learning set cannot fully represent the variability in
327 the whole dataset (1.5 million images). The average precision of the biological categories after
328 filtering was 84%. The trachymedusae and Acantharia radiolarians displayed the lowest
329 precision (61.9% and 65.4% respectively) but this already was an improvement of more than
330 50% compared to the situation before filtering.

331 To reach these precision levels, a large amount of images had to be discarded, leaving only
332 28.1% of the objects from the original dataset (n=39,758, excluding "noise" images). The
333 percentage of objects retained ranged from 8.5% for fibres (n=557) to a maximum of 63.7% for
334 solitary radiolarians (n=8,569). As a consequence, on average, filtering decreased recall by 39%
335 and F1 score by 7.8%. However, the improvement in precision dominated the effect of the
336 decrease in recall, because classification accuracy of the whole dataset improved from 40.2% to
337 56.3% after filtering.

338 **Table 2. Classification metrics before and after filtering out objects with low prediction**
 339 **confidence:** number of particles before filtering (n); percentage of data kept after filtering;
 340 precision, recall, and F1 score before and after filtering, and difference (after – before).
 341 Improvements (positive differences) are bolded. Non-living groups are presented first, groups of
 342 biological interest second.

Class	n	%kept	Precision			Recall			F1		
			before	after	diff	before	after	diff	before	after	diff
Dark aggregates	60164	6.5	77	95	19	50	7	-43	60	7	-54
Light aggregates	4209	4.2	8	17	9	53	4	-49	14	4	-10
Fibers	8055	6.9	46	85	38	56	7	-49	51	7	-44
Copepods	17459	22.4	54	88	34	72	22	-49	62	22	-39
Doliolids	30478	40.2	80	95	16	64	40	-24	71	40	-31
Fish larvae	802	23.2	12	80	67	62	23	-39	21	23	3
Trachymedusae	524	50.6	9	62	53	79	51	-29	16	51	35
Diatom chains	11015	28.6	75	97	22	72	29	-43	73	29	-45
Acantharia radiolarians	1021	18.9	7	65	58	74	19	-55	14	19	5
Radiolarian colonies	4367	16.7	24	94	70	62	17	-45	35	17	-18
Solitary radiolarians	13049	65.7	68	88	19	89	66	-23	77	66	-12
Shrimps	213	52.6	51	89	38	74	53	-21	60	53	-7

343 *Comparison of size spectra in the reference and predicted datasets*

344 In most classes, the size distribution of objects in the automatically predicted dataset and in the
 345 reference dataset were closely related (Figure 2). However, in three groups (fish larvae,
 346 radiolarian colonies, and shrimps), the shape of the spectrum was conserved but the occurrence
 347 of small objects was under-estimated. In particular, the mode of the spectrum (i.e. the most
 348 frequent size class) was larger by 1.3 mm for fish larvae in the predicted dataset compared to
 349 the reference dataset, by 6 mm for radiolarian colonies and by 2.8 mm for shrimps (Figure 2).

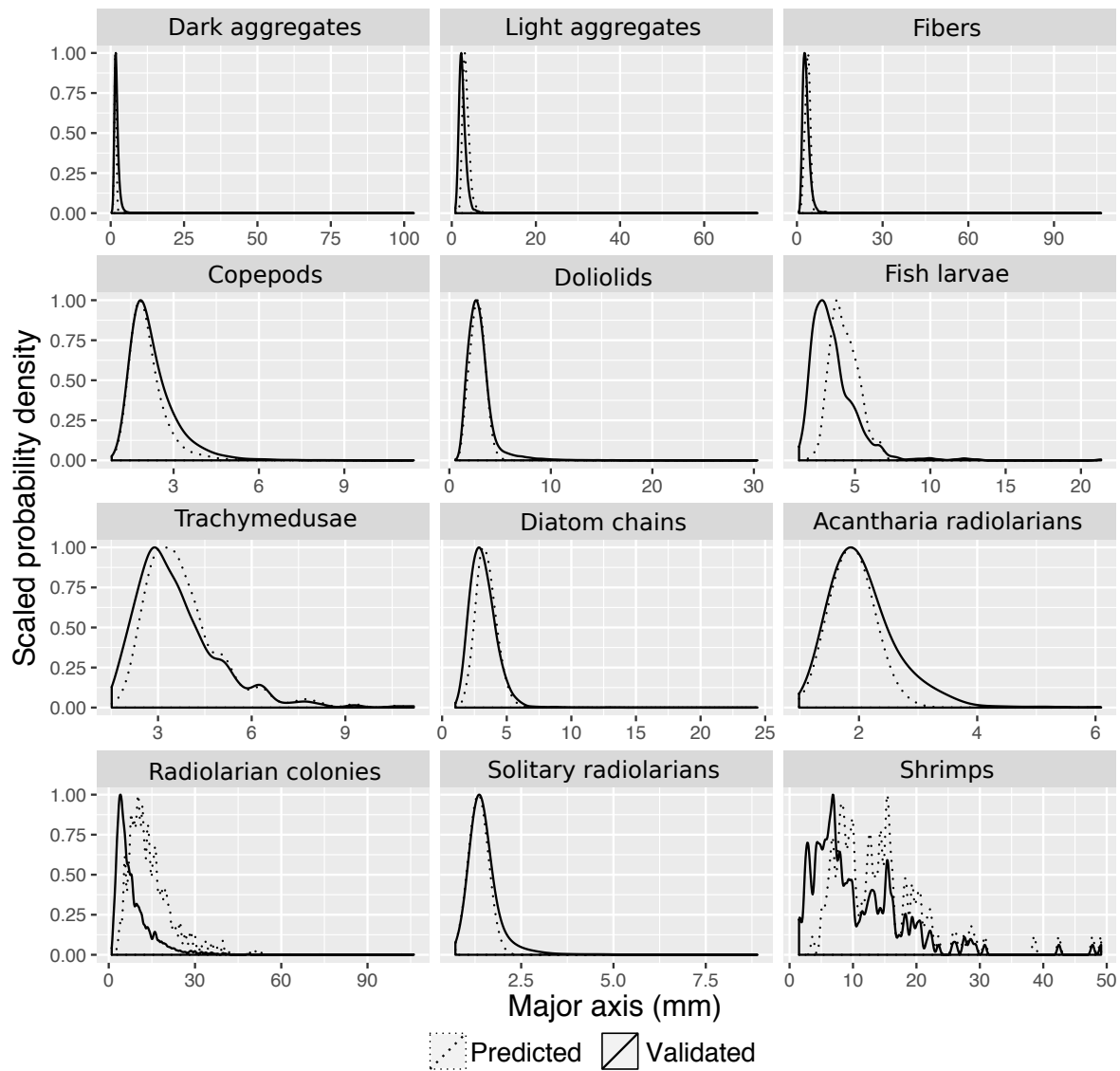


Figure 2. Per-class size spectra in the reference (solid lines) and automatically predicted and filtered (dotted lines) datasets. Probability density distributions of sizes were scaled between 0 and 1 to focus attention on the shapes of the distribution rather than the differences in the number of objects between the two datasets. The minimum size of objects considered was 250 pixels in area, resulting in $\geq 920 \mu\text{m}$ in major axis.

Distribution of plankton with respect to the front

The automatically predicted and filtered spatial distributions of most taxa and particles were significantly correlated with the reference distributions in 20 of the 22 groups at the $p < 0.001$

359 level (Table 3; Figure 3). Correlation coefficients were also very high (seven classes with $r > 0.7$,
 360 and eight additional classes with $r > 0.5$). The only two exceptions are fish larvae and shrimps in
 361 the day transect, both of which were very rare.

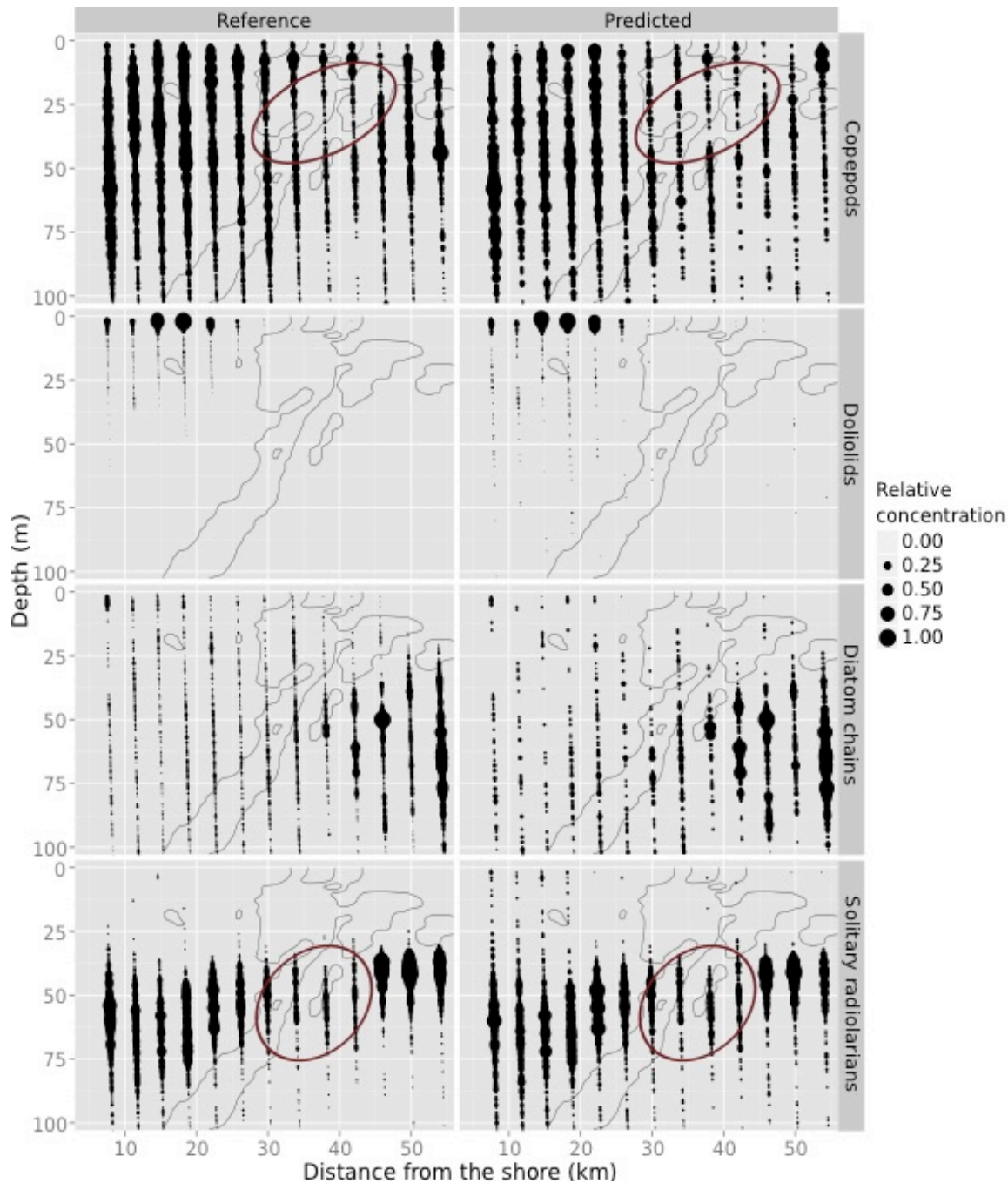
362 At the chosen 99%-precision filtering level, so many images of fish larvae and fibres were
 363 discarded that the resulting spatial distributions were very sparse (14.9% and 8.5% of images
 364 left, respectively; Figure 4). Such sparse distributions would clearly not be interpreted
 365 ecologically, given how little data are left and how much is discarded. So, information is lost but
 366 at least no wrong conclusions would be drawn. In addition, even in those cases, the locations of
 367 the maximum concentration zones were properly captured in the predicted dataset; there were
 368 just too few objects to represent the finer patterns (Figure 4).

369 **Table 3. Statistical comparisons of spatial distributions between the reference and predicted**
 370 **datasets with three statistics:** Dutilleul modified t -test (statistic, recomputed degrees of
 371 freedom and p -value), Pearson's correlation coefficient and Spearman's rank correlation
 372 coefficient. NB: no light aggregates were observed at night.

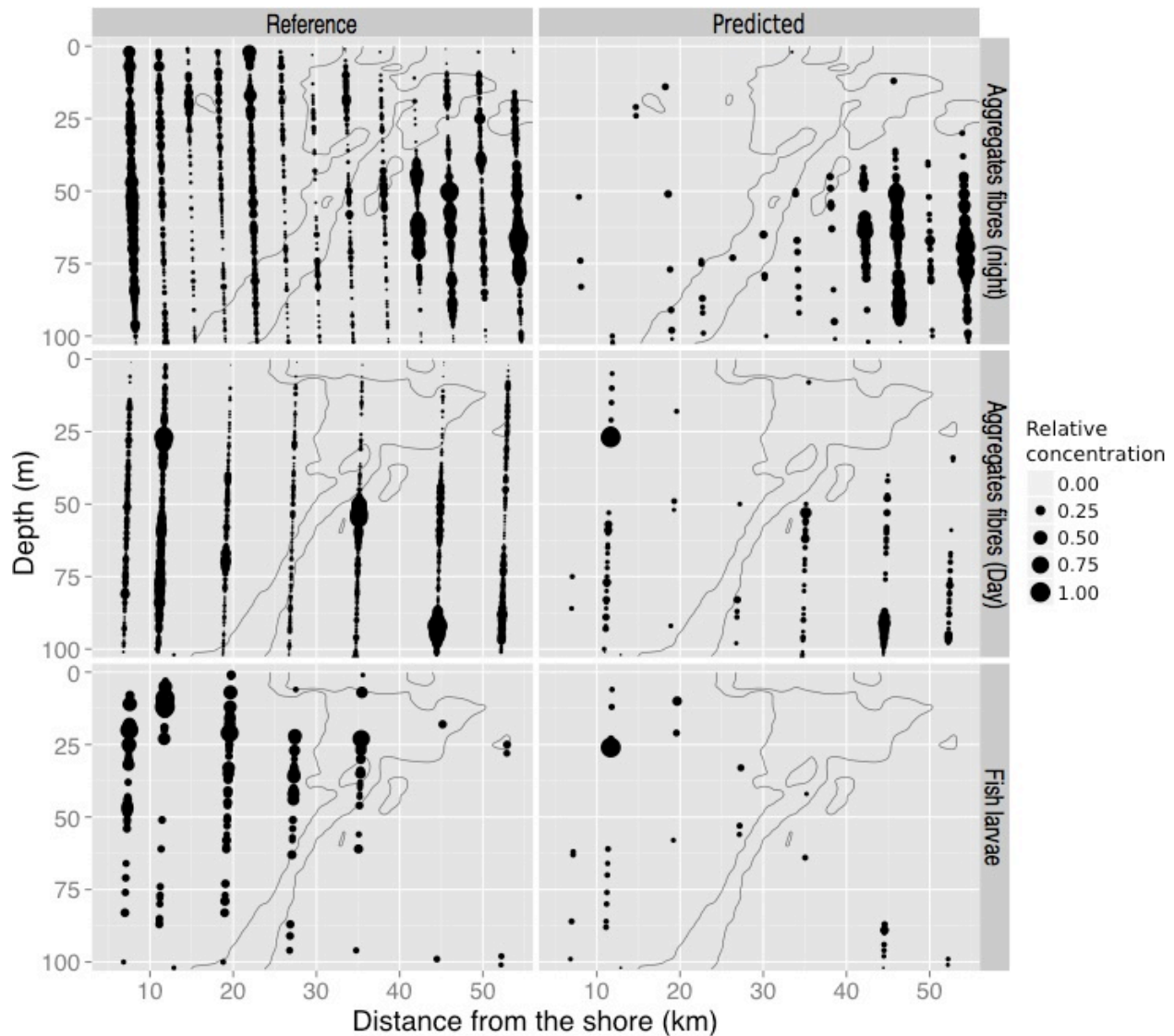
Class	Transect	Dutilleul t -test			Pearson's r	Spearman's rho
		F -stat	DoF	p -value		
Dark aggregates	Night	29.99	35	$p < 0.001$	0.66	0.68
	Day	24.11	20	$p < 0.001$	0.68	0.74
Light aggregates	Day	10.05	76	$p < 0.01$	0.11	0.34
Fibers	Night	103.22	155	$p < 0.001$	0.38	0.62
	Day	144.93	191	$p < 0.001$	0.42	0.62
Copepods	Night	54.37	36	$p < 0.001$	0.74	0.71
	Day	36.50	28	$p < 0.001$	0.73	0.71
Doliolids	Night	12244.11	275	$p < 0.001$	0.66	0.94
	Day	27064.77	187	$p < 0.001$	0.55	0.94
Fish larvae	Night	231.25	162	$p < 0.001$	0.44	0.77
	Day	1.58	561	0.21	0.09	0.05
Trachymedusae	Night	286.28	168	$p < 0.001$	0.61	0.78
	Day	130.66	287	$p < 0.001$	0.48	0.55
Diatom chains	Night	431.64	74	$p < 0.001$	0.72	0.92
	Day	377.12	97	$p < 0.001$	0.75	0.86

Acantharia radiolarians	Night	130.32	176	<i>p</i><0.001	0.53	0.64
	Day	107.86	167	<i>p</i><0.001	0.47	0.65
Radiolarian colonies	Night	220.39	358	<i>p</i><0.001	0.61	0.64
	Day	116.20	393	<i>p</i><0.001	0.52	0.49
Solitary radiolarians	Night	107.11	22.24	<i>p</i><0.001	0.91	0.89
	Day	101.06	14.33	<i>p</i><0.001	0.92	0.91
Shrimps	Night	685.26	893.08	<i>p</i><0.001	0.72	0.82
	Day	0.01	719.25	0.91	0.00	0.00

373 The reference spatial distributions showed that most taxa were strongly influenced by the
374 frontal zone: fish larvae, Acantharia radiolarians and doliolids were constrained on the coastal
375 side of the front, copepods were also more concentrated towards the coast and in the upper
376 layers of the water column, while diatom chains were more abundant in the deep, offshore
377 zones (Figure 3, left column). The high spatial resolution of the data allowed us to detect smaller
378 scale patterns such as a region of slightly lower concentrations of copepods and solitary
379 radiolarians at the front (around 30 m depth for copepods and 50 m depth for radiolarians;
380 Figure 3). Solitary radiolarians also occurred in shallower water in the offshore zone compared
381 to the coastal zone (Figure 3) and precisely followed the DCM (not mapped). All these patterns,
382 from the contrasts between taxa to the fine-scale low concentration regions at the front, could
383 also be well detected on the predicted data (Figure 3, right column). The ecological
384 interpretations in terms of the distribution relative to the frontal zone would be the same.



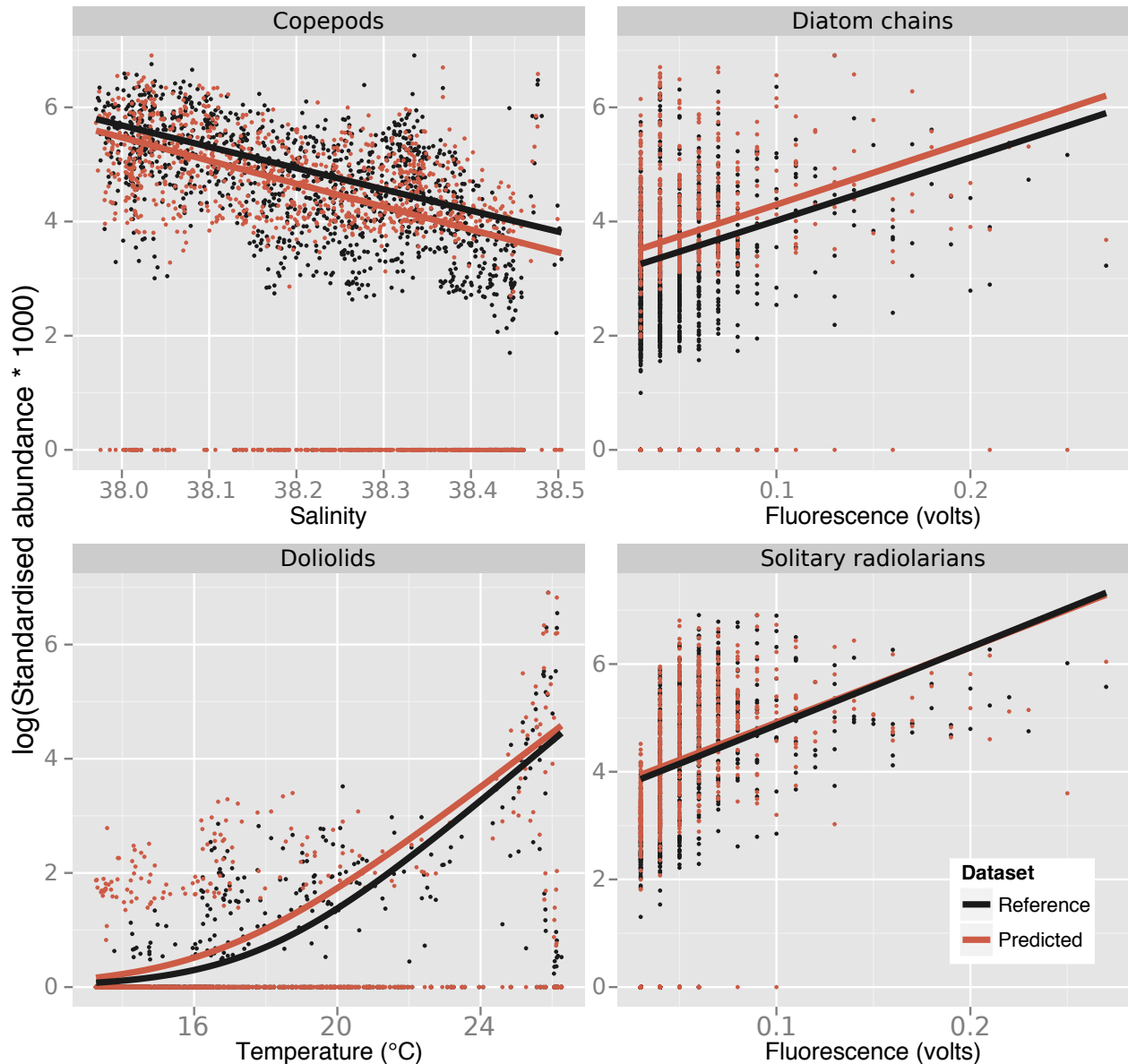
385 **Figure 3. Examples of some spatial distributions in the predicted dataset (right) that are well**
 386 **correlated with the reference dataset (left).** From top to bottom: copepods, doliolids,
 387 diatom chains and solitary radiolarians, all during the night transect. The x-axis is the distance from the
 388 coast (coastal side on the left, offshore side on the right). The area of the dots is proportional to
 389 the concentration, scaled to a maximum of 1 per taxon in each dataset, to ease comparison of
 390 patterns; the legend shows five examples but scaling is continuous. Grey lines are the 38.2 and
 391 38.3 isohalines that delineate the frontal region. Ellipses highlight regions of lower
 392 concentration located in the frontal zone.



393
 394 **Figure 4. Examples of poorly predicted spatial distributions (right) compared to the reference**
 395 **distributions (left).** From top to bottom: fibres at night, then during the day and fish larvae
 396 during the day. Same conventions as Figure 3.

397 The relationships between the abundance of biological taxa and various environmental
 398 variables (salinity, temperature, chlorophyll *a* fluorescence, oxygen concentration) were very
 399 similar in the reference and predicted datasets. In fact, in 69 of the 80 relationships that could
 400 be modelled with GLMs, the slopes were not significantly different between the two datasets.
 401 For example, copepods were more abundant in fresher waters (Figure 5), which were found on
 402 the coastal side of the front. The relationships with chlorophyll *a* fluorescence highlighted the

403 association of diatom chains and solitary radiolarians with the DCM. Finally, doliolids were vastly
404 more abundant in warmer, surface waters (Figure 5). All these conclusions would be reached
405 with the predicted dataset, which suggests that it could be used to explore and define the
406 habitat preference of various organisms.



407
408 **Figure 5. Examples of the influence of environmental variables on the distribution and**
409 **concentration of several taxa for the reference dataset (black) and automatically predicted**
410 **and filtered dataset (red).** The lines are the fitted values of GLMs with a Poisson distribution of
411 the residuals. The slopes of the GLM based on the predicted dataset are not significantly
412 different from the ones based on the reference dataset (ANOVA, all $p > 0.05$). Concentration is

413 standardised between groups based on the maximum concentration per taxa and per dataset.

414 *Day and night vertical distributions*

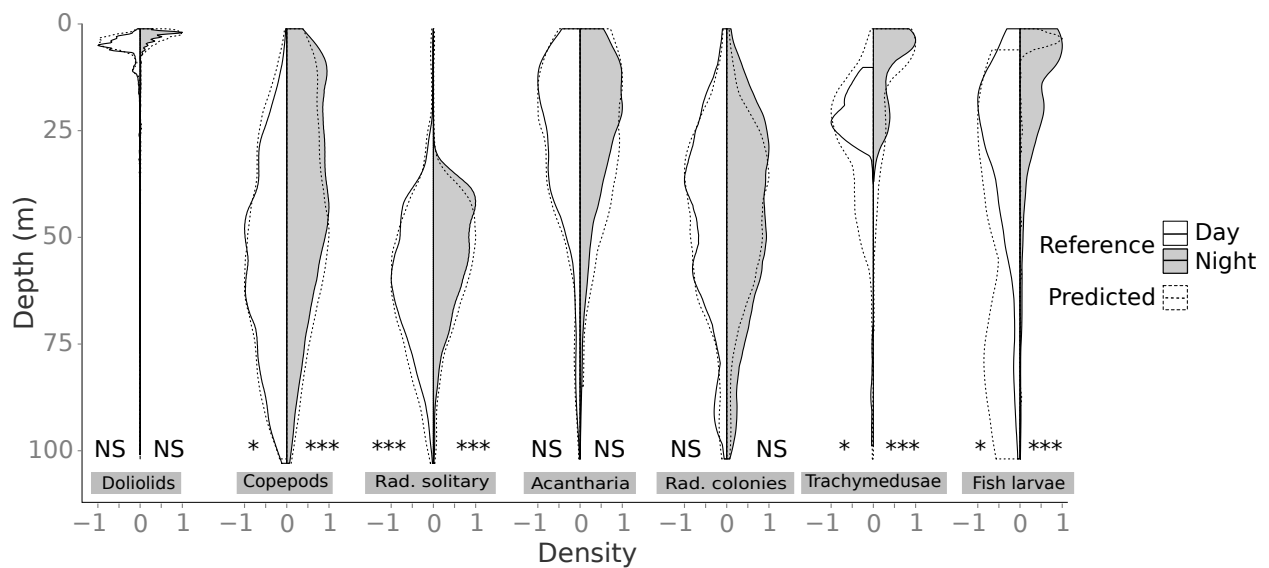
415 In 8 of 12 groups, the predicted and reference vertical distributions were slightly but
 416 significantly different (Solow-Kolmogorov-Smirnov test, $p < 0.05$; Table 4). The four groups in
 417 which the distributions were not statistically different were doliolids, Acantharia radiolarians,
 418 colonial radiolarians and shrimps, although the lack of significant difference in the latter group
 419 was probably due to their low overall numbers.

420 **Table 4. Statistical comparisons of vertical distributions between the reference and predicted**
 421 **datasets.** The statistic and p -value of the Solow-Kolmogorov-Smirnov test are reported, as well
 422 as the depth centre of mass of the distribution.

Class	Transect	Solow K-S		Depth (m)	
		K	p	Reference	Predicted
Dark aggregates	Day	3.22	<0.0001	49.1	55.3
	Night	3.91	<0.0001	41.2	53.1
Light aggregates	Day	2.98	<0.0001	29.0	40.5
	Night	3.97	<0.0001	51.5	69.3
Fibres	Day	1.61	0.0050	61.8	69.7
	Night	2.97	<0.0001	40.8	44.9
Copepods	Day	1.44	0.0250	56.1	55.1
	Night	0.67	0.5690	5.1	6.9
Doliolids	Day	0.82	0.3370	7.1	8.6
	Night	1.86	<0.0001	16.9	10.9
Fish larvae	Day	1.25	0.0490	32.6	52.2
	Night	1.44	0.0080	10.5	12.7
Trachymedusae	Day	1.31	0.0240	25.9	29.5
	Night	3.67	<0.0001	57.5	63.1
Diatom chains	Day	1.72	0.0010	64.3	67.8
	Night	1.13	0.1300	25.3	27.1
Acantharia radiolarians	Day	0.69	0.6070	28.3	29.9
	Night	1.20	0.0940	45.4	44.4

	Day	0.51	0.9020	45.8	46.3
Radiolarians solitary	Night	2.43	<0.0001	53.5	55.9
	Day	2.23	<0.0001	59.3	60.9
Shrimps	Night	1.00	0.1990	55.3	53.8
	Day	0.51	1.0000	49.9	44.1

423 For many groups, except trachymedusae and fish larvae, ecological conclusions regarding depth
 424 spread and preferendum would be the same in the reference and predicted dataset, even when
 425 distributions were statistically different (Table 4, column “Depth (m)” and Figure 4). Similarly, an
 426 analysis of diel vertical migration patterns would reach very similar conclusions on the reference
 427 and on the predicted dataset. When a significant diel vertical migration was detected in the
 428 reference dataset, it was also significant in the predicted one (Table 5). Conversely, radiolarian
 429 colonies and Acantharia radiolarians do not appear to vertically migrate and this conclusion was
 430 also reached with the predicted dataset. The range of downward migration of Trachymedusae,
 431 solitary radiolarians and doliolids were also very comparable between the datasets; the same
 432 was true, to a lesser extent, for calanoid copepods (Table 5, Figure 6). However, the vertical
 433 migration of fish larvae was poorly predicted, with a bias towards the surface at night that was
 434 much greater than in reality (Figure 6).



435
 436 **Figure 6. Examples of vertical distribution during the day (left side) and at night (right side,**
 437 **shaded) as depicted in the reference dataset (solid) and in the predicted and filtered dataset**

438 **(dashed)**. The significant levels of the comparisons between reference and predicted
439 distributions are indicated for both day and night (NS: not significant; *: $p < 0.05$; **: $p < 0.01$;
440 ***: $p < 0.001$).

441 **Table 5. Comparison of the resolution of diel vertical migration patterns in the reference and**
442 **predicted datasets.** Reported for each dataset are: (i) the statistic (K) of the Solow-Kolmogorov-
443 Smirnov test comparing day and night (bold when the test is significant), which quantifies the
444 overall difference in distribution, and (ii) the difference between the depth centre of mass at
445 night and during the day, a proxy for the migration range (night – day; negative means upward
446 migration at night).

	Solow-K-S day ~ night (K)		Migration range (m)	
	Reference	Predicted	Reference	Predicted
Copepods	4.10	2.86	-15.3	-10.3
Doliolids	1.16	1.14	-2.1	-1.7
Fish larvae	1.88	1.72	-15.8	-41.4
Trachymedusae	1.72	2.07	-15.4	-16.8
Diatom chains	2.53	2.25	-6.8	-4.7
Acantharia radiolarians	0.99	1.15	-3.0	-2.9
Radiolarian colonies	0.50	0.67	-0.4	-1.9
Solitary radiolarians	3.04	2.75	-5.8	-5.0
Shrimps	0.83	0.81	5.4	9.6

447 **DISCUSSION**

448 The method presented here aimed at bypassing the manual validation of predicted
449 identifications by discarding objects classified with low confidence, hence improving precision
450 (but decreasing recall). The precision increase (+37% on average) was counter-balanced by a
451 recall decrease (-39% on average), but overall classification accuracy using this method
452 increased by 16%.

453 The quality and resolution of images may influence the maximum taxonomic resolution

454 achievable by any automatic classification method. Studies based on high quality laboratory
455 imagery of plankton have usually reached higher accuracy and could resolve a larger number of
456 groups (e.g. 22 phytoplankton groups in Sosik and Olson (2007); 25 zooplankton groups in
457 Fernandes et al. (2009); 10-20 groups in Benfield et al., 2007) than studies based on images of
458 zooplankton captured *in situ* which are usually of lesser quality (e.g. three groups with SVM,
459 achieving 80% accuracy (Bi et al., 2015); seven groups with random subspace model achieving
460 >90% precision but in a self-prediction of the learning set (Zhao et al., 2010); five to seven
461 groups with neural networks, reaching 60 to 80% accuracy; Davis et al., 2004; Hu and Davis,
462 2005). While only a formal comparison, using the same dataset (e.g. Fei-Fei et al. 2007), could
463 resolve the differences between classification methods, comparing the size orders of
464 classification metrics between studies can still be informative. Here, our classifier dealt with 14
465 groups and, after filtering, reached 56.3% general accuracy as well as 84% precision on
466 biological groups. This falls within the higher range in terms of precision and number of
467 predicted groups compared to previous studies on *in situ* images of zooplankton, especially
468 considering that 67-83% accuracy is often used as a benchmark for plankton classifications
469 (Culverhouse et al., 2003; Hu and Davis, 2005). While there is still room for improvement in the
470 original classification rates, the data filtering method presented in this study markedly improved
471 the performance of the standard *ZooProcess/PkID* classification.

472 Large image datasets are likely to become increasingly common thanks to the development of
473 affordable high-frequency, high-resolution cameras like the one installed on ISIS. In such big
474 datasets, all the information may not be essential and some may be efficiently omitted (Bi et al.,
475 2015). The filtering approach used in this study considerably subsampled the data (72% of
476 objects were discarded) in order to focus only on well-predicted objects. Despite this high
477 subsampling rate, the two dimensional, and to a lesser extent vertical, distributions of many
478 classes were not significantly different between the subsampled and the total, reference
479 dataset. In addition, the poorly predicted groups could be easily identified by the sparseness of
480 their predicted distribution and/or the high proportion of discarded images (>90%). This
481 provided an additional control for the validation of automatically predicted distributions.

482 More importantly, studying realistic ecological questions with the reference and predicted
483 datasets resulted in the same conclusions.

484 The size distribution of objects of most classes (9 of 12) were similarly represented in both the
485 automatically predicted and filtered dataset (Figure 2). In the three other classes, the filtering
486 method discarded small objects (<5 mm) more often than larger ones, possibly because small
487 objects are more prone to be misclassified due to their lower level of detail.

488 The results also highlighted the foremost influence of the frontal structure, marked by a salinity
489 gradient, on the distributions of organisms along the across-front section (Figure 5). This is
490 consistent with many studies from the literature (Boucher, 1984; Goffart et al., 1995; Pedrotti
491 and Fenaux, 1992). For example, some taxa like Acantharia radiolarians, doliolids, fish larvae,
492 and, to a lesser extent, copepods were mostly observed in the coastal or frontal zones and in
493 the upper 50 m of the water column (Figures 3 and 4). Both datasets allowed us to relate the
494 abundance of various taxa to the salinity gradient, which marks the frontal region, the intensity
495 of the fluorescence of chlorophyll *a* associated with the DCM, or the warmer temperatures
496 found near the surface (Figure 5). Overall, 86% of the relationships with environmental variables
497 that were explored were not statistically different between the two datasets. Finally, diatom
498 chains were most abundant in the deeper layers of the central zone, where copepod
499 concentrations were the lowest (Figure 3), suggesting a possible influence of grazing. These
500 results suggest that species-environment relationships or interspecific interactions can be
501 studied at the very fine scales that imaging techniques provide without requiring labour-
502 intensive validation.

503 Changes in vertical distributions between day and night, even over less than 10 m, could also be
504 detected in the predicted data for most taxa, with a power and resolution similar to that of the
505 reference dataset (Figure 6; Table 4). Diel vertical migrations of copepods and medusae are well
506 described in the literature (e.g. Hays, 2003; Sabatés et al., 2010). However, the apparent <10 m
507 vertical movements of solitary Colodaria radiolarians or the 2 m downward displacement of
508 doliolids during the day are not documented in prior studies, possibly because they were missed
509 by other sampling methods with lower vertical resolutions. The ecological significance of these

510 fine scale vertical movements is not within the scope of this study, but the fact that they could
511 be detected highlights the efficacy of both high frequency imaging systems and this automatic
512 classification and filtration method in exploring microscale processes in the plankton.

513 Nonetheless, some taxa share striking similarities and only a trained expert may be able to
514 differentiate between them. These size and shape resemblances can lead to high error rates in
515 the automatic prediction of these groups (Fernandes et al., 2009). Automatic classification
516 methods may never reach the taxonomical resolution achieved by experts observing plankton
517 through a stereomicroscope (even if both make mistakes; Culverhouse et al., 2003). Still,
518 combined with data filtering, automatic classification can accurately describe spatial
519 distributions when low taxonomical resolution is acceptable, for example to study broad groups
520 that provide an environmental or biological context for a species of interest. Eventually, manual
521 validation is likely to still be required in order to focus on some specific taxonomic group. For
522 example, fish larvae imaged here were very diverse and appeared similar to appendicularians
523 and chaetognaths in terms of body size, shape and opacity. As a result, this group was badly
524 predicted and manual methods would still be necessary to tease apart their distribution.

525 Using the proposed method, the processing of 1.5 million objects required only the manual
526 classification of 5979 objects (0.41%). It could properly describe distribution patterns, but the
527 drastic filtering process would lead to vastly underestimating the abundances of all groups. In
528 future studies, these underestimated abundances could be scaled up by quantifying, in each
529 class, the proportion of discarded and wrongly classified objects (e.g. with a confusion matrix).
530 This quantification requires to manually validate a random subset of images of each category of
531 the predicted dataset, thus requiring additional human effort. However, during validation of the
532 1.5 million in this project, the throughput of a trained operator was about 10,000 objects per
533 day. Therefore, human effort on the order of a couple of weeks would probably yield enough
534 data to correct abundances and further control the error rate for the rest of the predicted
535 images.

536 The present method is based on two features shared by all machine learning methods: the use
537 of a learning set to teach the model how to differentiate between classes and the computation

538 of a final score, or probability, for each object to belong in each class. The probability thresholds
539 for the filtering step are computed by cross-validating the learning set and do not require
540 additional manual sorting. In many cases, Random Forest, working on a few dozen features
541 deterministically measured on the object, came out as the most efficient classifier for plankton
542 data (e.g. Bell and Hopcroft, 2008; Fernandes et al., 2009; Gorsky et al., 2010). Yet, overall
543 accuracy was never more than 80%. However, deep machine learning methods such as
544 convolutional neural networks (CNNs) are emerging as promising tools for a range of image
545 classification tasks (Krizhevsky et al., 2012; Simonyan and Zisserman, 2015). Applying the
546 filtering method described here to classifiers that already achieve high accuracy on large
547 datasets may eventually lead to near-perfect automatic classifications, without discarding too
548 much information. Such a combination would allow the handling of large plankton imaging
549 datasets that are still challenging to process rapidly and accurately (Benfield et al., 2007;
550 Culverhouse et al., 2006), hence providing appropriate tools to explore the finescale and
551 microscale processes occurring in the oceans.

552 **ACKNOWLEDGMENTS**

553 The authors thank A. Maupetit and F. Ferrando for their help with the manual identification, the
554 crew of the R/V Tethys 2 operating during the *VISUFRONT* cruise and CNRS/INSU for the ship
555 time. This work was supported by a grant from the Partner University Fund to JOI and RKC. RF's
556 doctoral fellowship was provided by the French Ministry for Education and Research (n^o
557 247/2012).

558 **REFERENCES**

559 Bakun, A., 2006. Fronts and eddies as key structures in the habitat of marine fish larvae :
560 opportunity , adaptive response. *Sci. Mar.* 105–122.

561 Belkin, I.M., 2002. *Front. Interdiscip. Encycl. Mar. Sci.*

562 Belkin, I.M., Cornillon, P.C., Sherman, K., 2009. *Fronts in Large Marine Ecosystems. Prog.*
563 *Oceanogr.* 81, 223–236.

564 Bell, J.L., Hopcroft, R.R., 2008. Assessment of Zoolmage as a tool for the classification of
565 zooplankton. *J. Plankton Res.* 30, 1351–1367.

566 Benfield, M., Grosjean, P., Culverhouse, P., Irigolen, X., Sieracki, M., Lopez-Urrutia, A., Dam, H.,
567 Hu, Q., Davis, C., Hanson, A., Pilskaln, C., Riseman, E., Schulz, H., Utgoff, P., Gorsky, G.,
568 2007. RAPID: Research on Automated Plankton Identification. *Oceanography* 20, 172–187.

569 Benfield, M.C., Davis, C.S., Wiebe, P.H., Gallager, S.M., Gregory Loughj, R., Copley, N.J., 1996.
570 Video Plankton Recorder estimates of copepod, pteropod and larvacean distributions from
571 a stratified region of Georges Bank with comparative measurements from a MOCNESS
572 sampler. *Deep. Res. Part II Top. Stud. Oceanogr.* 43, 1925–1945.

573 Benoit-Bird, K.J., McManus, M.A., 2012. Bottom-up regulation of a pelagic community through
574 spatial aggregations. *Biol. Lett.* 8, 813–816.

575 Bi, H., Cook, S., Yu, H., Benfield, M.C., Houde, E.D., 2013. Deployment of an imaging system to
576 investigate fine-scale spatial distribution of early life stages of the ctenophore *Mnemiopsis*
577 *leidyi* in Chesapeake Bay. *J. Plankton Res.* 35, 270–280.

578 Bi, H., Guo, Z., Benfield, M.C., Fan, C., Ford, M., Shahrestani, S., Sieracki, J.M., 2015. A Semi-
579 Automated Image Analysis Procedure for In Situ Plankton Imaging Systems. *PLoS One* 10,
580 e0127121.

581 Boucher, J., 1984. Localization of zooplankton populations in the Ligurian marine front: role of
582 ontogenic migration. *Deep Sea Res.* 31, 469–484.

583 Boucher, J., Ibanez, F., Prieur, L., 1987. Daily and seasonal variations in the spatial distribution of
584 zooplankton populations in relation to the physical structure in the Ligurian Sea Front. *J.*
585 *Mar. Res.* 45, 133–173.

- 586 Breiman, L., 2001. Random Forests. *Mach. Learn.* 45, 5–32.
- 587 Cowen, R.K., Greer, A.T., Guigand, C.M., Hare, J.A., Richardson, D.E., Walsh, H.J., 2013.
588 Evaluation of the In Situ Ichthyoplankton Imaging System (ISIS): comparison with the
589 traditional (bongo net) sampler. *Fish. Bull.* 111, 1–12.
- 590 Cowen, R.K., Guigand, C.M., 2008. In situ ichthyoplankton imaging system (ISIS): system design
591 and preliminary results. *Limnol. Oceanogr. Methods* 6, 126–132.
- 592 Culverhouse, P.F., Williams, R., Benfield, M., Flood, P.R., Sell, A.F., Mazzocchi, M.G., Buttino, I.,
593 Sieracki, M., 2006. Automatic image analysis of plankton: Future perspectives. *Mar. Ecol.*
594 *Prog. Ser.* 312, 297–309.
- 595 Culverhouse, P.F., Williams, R., Reguera, B., Herry, V., González-Gil, S., 2003. Do experts make
596 mistakes? A comparison of human and machine identification of dinoflagellates. *Mar. Ecol.*
597 *Prog. Ser.* 247, 17–25.
- 598 Davis, C.S., Gallager, S.M., Solow, A.R., 1992. Microaggregations of oceanic plankton observed
599 by towed video microscopy. *Science.* 257, 230–232.
- 600 Davis, C.S., Hu, Q., Gallager, S.M., Tang, X., Ashjian, C.J., 2004. Real-time observation of taxa-
601 specific plankton distributions: An optical sampling method. *Mar. Ecol. Prog. Ser.* 284, 77–
602 96.
- 603 Dutilleul, P., Clifford, P., Richardson, S., Hemon, D., 1993. Modifying the t Test for Assessing the
604 Correlation Between Two Spatial Processes. *Biometrics* 49, 305.
- 605 Espinasse, B., Zhou, M., Zhu, Y., Hazen, E.L., Friedlaender, A.S., Nowacek, D.P., Chu, D., Carlotti,
606 F., 2012. Austral fall-winter transition of mesozooplankton assemblages and krill
607 aggregations in an embayment west of the Antarctic Peninsula. *Mar. Ecol. Prog. Ser.* 452,
608 63–80.
- 609 Fei-Fei, L., Fergus, R., Perona, P., 2007. Learning generative visual models from few training
610 examples: An incremental bayesian approach tested on 101 object categories. *Comput. Vis.*

611 Image Underst. 106, 59–70.

612 Fernandes, J.A., Irigoien, X., Boyra, G., Lozano, J.A., Inza, I., 2009. Optimizing the number of
613 classes in automated zooplankton classification. *J. Plankton Res.* 31, 19–29.

614 Gasparini, S., Antajan, E., 2013. PLANKTON IDENTIFIER: a software for automatic recognition of
615 planktonic organisms.

616 Goffart, A., Hecq, J.-H., Prieur, L., 1995. Controle du phytoplancton du bassin Ligure par le front
617 liguro-provencal (secteur Corse). *Oceanol. Acta* 18, 329–342.

618 Gorsky, G., Ohman, M.D., Picheral, M., Gasparini, S., Stemmann, L., Romagnan, J.B., Cawood, A.,
619 Pesant, S., García-Comas, C., Prejger, F., 2010. Digital zooplankton image analysis using the
620 ZooScan integrated system. *J. Plankton Res.* 32, 285–303.

621 Greer, A.T., Cowen, R.K., Guigand, C.M., Hare, J.A., 2015. Fine-scale planktonic habitat
622 partitioning at a shelf-slope front revealed by a high-resolution imaging system. *J. Mar.*
623 *Syst.* 142, 111–125.

624 Greer, A.T., Cowen, R.K., Guigand, C.M., Hare, J.A., Tang, D., 2014. The role of internal waves in
625 larval fish interactions with potential predators and prey. *Prog. Oceanogr.* 127, 47–61.

626 Greer, A.T., Cowen, R.K., Guigand, C.M., McManus, M.A., Sevadjian, J.C., Timmerman, A.H. V.,
627 2013. Relationships between phytoplankton thin layers and the fine-scale vertical
628 distributions of two trophic levels of zooplankton. *J. Plankton Res.* 35, 939–956.

629 Grimes, C.B., Finucane, J.H., 1991. Spatial distribution and abundance of larval and juvenile fish,
630 chlorophyll and macrozooplankton around the Mississippi River discharge plume, and the
631 role of the plume in fish recruitment. *Mar. Ecol. Prog. Ser.* 75, 109–119.

632 Hays, G.C., 2003. A review of the adaptive significance and ecosystem consequences of
633 zooplankton diel vertical migrations. *Hydrobiologia* 503, 163–170.

634 Herman, A.W., Mitchell, M.R., Young, S.W., 1984. A continuous pump sampler for profiling

635 copepods and chlorophyll in the upper oceanic layers. *Deep Sea Res.* 31, 439–450.

636 Hu, Q., Davis, C., 2005. Automatic plankton image recognition with co-occurrence matrices and
637 Support Vector Machine. *Mar. Ecol. Prog. Ser.* 295, 21–31.

638 Irisson, J.-O., Paris, C.B., Guigand, C., Planes, S., 2010. Vertical distribution and ontogenetic
639 “migration” in coral reef fish larvae. *Limnol. Oceanogr.* 55, 909–919.

640 Krizhevsky, A., Sutskever, I., Hinton, G.E., 2012. ImageNet Classification with Deep Convolutional
641 Neural Networks. *Adv. Neural Inf. Process. Syst.* 1–9.

642 Legendre, L., Le Fèvre, J., 1991. From Individual Plankton Cells To Pelagic Marine Ecosystems
643 And To Global Biogeochemical Cycles, in: Demers, S. (Ed.), *Particle Analysis in*
644 *Oceanography SE - 11, NATO ASI Series.* Springer Berlin Heidelberg, pp. 261–300.

645 Li, Z., Member, S., Zhao, F., Liu, J., Member, S., Qiao, Y., 2014. Pairwise Nonparametric
646 Discriminant Analysis for Binary Plankton Image Recognition. *IEEE J. Ocean. Eng.* 39, 695–
647 701.

648 Lough, R.G., Broughton, E.A., 2007. Development of micro-scale frequency distributions of
649 plankton for inclusion in foraging models of larval fish, results from a Video Plankton
650 Recorder. *J. Plankton Res.* 29, 7–17.

651 Luo, J., Grassian, B., Tang, D., Irisson, J., Greer, A., Guigand, C., McClatchie, S., Cowen, R., 2014.
652 Environmental drivers of the fine-scale distribution of a gelatinous zooplankton community
653 across a mesoscale front. *Mar. Ecol. Prog. Ser.* 510, 129–149.

654 MacLeod, N., Benfield, M., Culverhouse, P., 2010. Time to automate identification. *Nature* 467,
655 154–155.

656 McClatchie, S., Cowen, R., Nieto, K., Greer, A., Luo, J.Y., Guigand, C., Demer, D., Griffith, D.,
657 Rudnick, D., 2012. Resolution of fine biological structure including small narcomedusae
658 across a front in the Southern California Bight. *J. Geophys. Res.* 117, C04020.

659 Neilson, J.D., Perry, R.I., 1990. Diel vertical migrations of marine fishes: an obligate or facultative
660 process? *Adv. Mar. Biol.* 26, 115–168.

661 Olson, D.B., Hitchcock, G.L., Mariano, A.J., Ashjian, C.J., Peng, G., Nero, R.W., Podesta, G.P.,
662 1994. Life on the edge: marine life and fronts. *Oceanography* 7, 52–60.

663 Pedrotti, M.L., Fenaux, L., 1992. Dispersal of echinoderm larvae in a geographical area marked
664 by upwelling (Ligurian Sea, NW Mediterranean). *Mar. Ecol. Prog. Ser.* 86, 217–227.

665 Picheral, M., Guidi, L., Stemmann, L., Karl, D., Iddaoud, G., Gorsky, G., 2010. The Underwater
666 Vision Profiler 5: An advanced instrument for high spatial resolution studies of particle size
667 spectra and zooplankton. *Limnol. Oceanogr. Methods* 8, 462–473.

668 Pinel-Alloul, B., 1995. Spatial heterogeneity as a multiscale characteristic of zooplankton
669 community, in: *Space Partition within Aquatic Ecosystems*. Springer, pp. 17–42.

670 Sabatés, A., Pagès, F., Atienza, D., Fuentes, V., Purcell, J.E., Gili, J.M., 2010. Planktonic cnidarian
671 distribution and feeding of *Pelagia noctiluca* in the NW Mediterranean Sea. *Hydrobiologia*
672 645, 153–165.

673 Sammari, C., Millot, C., Prieur, L., 1995. Aspects of the seasonal and mesoscale variabilities of
674 the Northern Current in the western Mediterranean Sea inferred from the PROLIG-2 and
675 PROS-6 experiments. *Deep Sea Res. Part I Oceanogr. Res. Pap.* 42, 893–917.

676 Samson, S., Hopkins, T., Remsen, A., Langebrake, L., Sutton, T., Patten, J., 2001. A system for
677 high-resolution zooplankton imaging. *IEEE J. Ocean. Eng.* 26, 671–676.

678 Simonyan, K., Zisserman, A., 2015. Very Deep Convolutional Networks for Large-Scale Image
679 Recognition. *Intl. Conf. Learn. Represent.* 1–14.

680 Smeti, H., Pagano, M., Menkes, C., Lebourges-Dhaussy, A., Hunt, B.P., Allain, V., Rodier, M., de
681 Boissieu, F., Kestenare, E., Sammari, C., 2015. Spatial and temporal variability of
682 zooplankton off New Caledonia (Southwestern Pacific) from acoustics and net
683 measurements. *J. Geophys. Res. Ocean.* 120, 1–25.

684 Solow, A.R., Bollens, S.M., Beet, A., 2000. Comparing two vertical plankton distributions. *Limnol.*
685 *Oceanogr.* 45, 506–509.

686 Sosik, H.M., Olson, R.J., 2007. Automated taxonomic classification of phytoplankton sampled
687 with imaging in-flow cytometry. *Limnol. Oceanogr. Methods* 5, 204–216.

688 Vandromme, P., Stemmann, L., Berline, L., Gasparini, S., Mousseau, L., Prejger, F., Passafiume,
689 O., Guarini, J.-M., Gorsky, G., 2011. Inter-annual fluctuations of zooplankton communities
690 in the Bay of Villefranche-sur-mer from 1995 to 2005 (Northern Ligurian Sea, France).
691 *Biogeosciences* 8, 3143–3158.

692 Wiebe, P.H., Benfield, M.C., 2003. From the Hensen net toward four-dimensional biological
693 oceanography. *Prog. Oceanogr.* 56, 7–136.

694 Ye, L., Chang, C.Y., Hsieh, C.H., 2011. Bayesian model for semi-automated zooplankton
695 classification with predictive confidence and rapid category aggregation. *Mar. Ecol. Prog.*
696 *Ser.* 441, 185–196.

697 Zhao, F., Lin, F., Seah, H.S., 2010. Binary SIPPER plankton image classification using random
698 subspace. *Neurocomputing* 73, 1853–1860.

699